

Conductivity and Structure of Poly(ethylene glycol) Complexes Using Energy Dispersive X-ray Diffraction

R. Caminiti,^{*,†} M. Carbone,[‡] S. Panero,[†] and C. Sadun[†]

Dipartimento di Chimica, Istituto Nazionale di Fisica della Materia, Università di Roma "La Sapienza", P.le A. Moro 5, 00185 Roma, Italy, and Dipartimento di Scienze Chimiche e Tecnologia, Università "Tor Vergata", Via della Ricerca Scientifica 1, 00133 Roma, Italy

Received: April 22, 1999

Triflate salts of Mg(II), Zn(II), and Cu(II) in liquid, low weight poly(ethylene glycol) dimethyl ether (PEGM-400) to determine their conductivity and to ascertain their possible use as electrolyte media, have been studied. Their liquid structures have been studied by energy-dispersive X-ray diffraction. By this technique, the cation geometrical coordination has been determined. Furthermore, the local structure of the bivalent cations has been singled out by application of the difference method to isomorphous solutions. We found that the investigated cations have an octahedral coordination, with the exception of Cu, which displays two apical bonds longer than the planar ones. We also found that the polymer chain is coordinated to the cations Mg and Zn through the oxygen atoms of the polymer units 1, 5, and 9.

Introduction

For a long time, polymer electrolyte materials formed by incorporating inorganic salts into ion-coordinating polymers have been studied.^{1–9} They are very interesting electrochemical supports, since they offer good conductivity even if they keep the characteristic properties of plastic materials.¹⁰ The high and medium molecular weight poly(ethylene oxide) (PEO) has been one of the most studied polymers because of its exceptional aptitude to solvate ionic salts. It has been studied in relation to various monovalent, bivalent, and trivalent cations, associated with various anions, such as halogens, perchlorates, and triflates.

These solid systems show a multiphase structure (constituted by an amorphous phase, a pure crystalline PEO phase and a crystalline complex phase) that hampers their structural study. It represents a negative aspect for the conductivity; in fact, these systems achieve high conductivity at about 100 °C and suffer from low conductivity below 65 °C because of high crystallinity.

The possibility of introducing plasticizer,¹¹ in order to reduce the crystallinity at low temperatures, has been studied. A low molecular weight liquid system, constituted by the same PEO monomer unit, has been added to the solid systems.

Hence, the study of polyelectrolytic systems has been extended to low molecular weight PEO parent systems, which give rise to completely amorphous multivalent salt solutions. The hypothesis is that these "model solutions" are able to represent the more complex long chain systems, as far as the electric conductivity and the solute solvent interactions, from a structural point of view, are concerned. Poly(ethylene glycol) (PEG), and poly(ethylene glycol) dimethyl ether (PEGM) oligomers have been principally used. They, with multivalent salts, give rise to slightly more viscous liquid solutions with a good concentration of metal:ether oxygen atoms ratio up to 1:10.¹² These solutions can be more easily studied than the PEO-based solutions, provided they maintain, at a microscopic level,

similar behaviors, and they can give a general model of the cations mobility in the polymeric media.

Knowledge of the structure, as in many other areas of material science, is an essential foundation to build an understanding of the physical behavior, that is, in this particular case, the mechanism of ionic conductivity in complexes of polyethers.

The transport mechanism for ions in polymeric electrolytes is highly dependent on the polymer host and on the ion type. The considered properties for the optimizations of these electrolytes are (1) number and mobility of doping ions and (2) flexibility of polymeric host.

In high molecular weight systems, the dynamic bond percolation model¹³ describes long-range cation transport. This model is only valid for cations forming rather weak bonds with the ether oxygen of the polymer chain. In low molecular weight polymer systems such as PEG, the self-diffusion of the polymer chains to which the cation is attached¹⁴ gives an important contribution to cation transport. The difference in the transport mechanism between anions and cations is due to the much weaker interaction of the anions with the ether oxygen: the anions are believed to move between the voids in the polymer matrix.¹⁵ These factors include the interaction of the cation with the polymer, ionic association, and polymer segmental motion. They are not independent; for example, the interaction of the cation with the ether oxygen atoms of the polymer backbone decreases the polymer segmental motion, as seen in the increase of the glass transition temperature with increasing salt concentration. It is also expected that the various anion–cation interactions, which define the ionic association in the complex, be mediated by the interactions of the cations with the ether oxygen atoms.

The local structure surrounding the cation as defined by the coordinating ether oxygen atom has been studied using various techniques. The most suitable technique for the determination of the metal coordination geometry is X-ray diffraction, which is particularly useful also for liquid samples.

No structural studies about these solutions have been performed so far; only structural hypotheses have been made

* Corresponding author. E-mail: r.caminiti@caspur.it.

[†] Università di Roma "La Sapienza".

[‡] Università "Tor Vergata".

TABLE 1: Compositions of Some Polymer Electrolytes

solution	density (g cm ⁻³)	concn (m)
PEG ₂₀ -LiCF ₃ SO ₃	0.977	1.135
PEG ₂₀ -Cu(CF ₃ SO ₃) ₂	1.282	1.132
PEG ₂₀ -Zn(CF ₃ SO ₃) ₂	1.278	1.134
PEG ₂₀ -Mg(CF ₃ SO ₃) ₂	1.213	1.135

through the IR band shifts caused by the ether oxygen of the polymer chains, whether involved in the metal coordination or not. Eventually, there are no other studies involving metals such as Cu, Zn, and Mg. In this study we present the structural determination of Mg, Zn, and Cu triflate salts in PEGM (400) liquid solutions.

The properties of conductive polymers strongly depend on parameters such as the degree of cation solvation by the polymer, responsible for the mobility of the cation in solution, and the formation of ionic pairs in the solutions. The structural determination of the degree of association in solution is, therefore, important since it can give hints on the conduction mechanism.

In the present study, we have proposed a complete structure for the solvated cation Mg and Zn; i.e., not only has the cation coordination been determined but also we have found how the polymer chains wrap the cations.

To achieve the goal, we have used the “difference method”.¹⁶ Solutions of different salts with the same concentration have been prepared. Subtracting the radial distribution function of different solutions, one to the other, the only contributions refer to the metal interactions provided the two metals are isomorphous.

Experimental Section

Material. The end-capped (methyl groups) poly(ethylene glycol), 400 MW, (PEGM(400)) was purchased from Fluka, and it was used without further purification. The multination triflate salts, namely Cu(CF₃SO₃)₂, Zn(CF₃SO₃)₂, and Mg(CF₃SO₃)₂, Fluka products, were dried prior to use.

The PEG_x-M(CF₃SO₃)₂ solutions (where $x = 20$ is the ratio between the oxygen atoms in the ether and the cations from the salt and M stands for Zn, Cu, Mg) were prepared in a controlled atmosphere by directly dissolving the suitable amount of salts into the liquid PEGM and by subsequent stirring until homogenization was achieved. A PEGM₂₀-LiCF₃SO₃ solution has been also prepared and characterized in comparison. Elemental analysis was performed by atomic absorption with a Varian Spectra AA30 instrument. Table 1 reports the data relating to the polymeric solutions used in this work.

Techniques. 1. Conductivity. The conductivity measurements were carried out by impedance spectroscopy (65 kHz to 10 Hz) using the Solarton Model 1250 frequency response analyzer, controlled by a desktop computer. A glass cell with two Pt blocking electrodes was used for measurements.

2. X-ray Diffraction. The X-ray diffraction experiments were carried out by employing a noncommercial X-ray energy scanning diffractometer.^{17,18} The diffractometer is constituted by an X-ray generator (water-cooled W target, with 3.0 kW maximum power), a solid-state detector (SSD), connected to a multichannel analyzer by an electronic chain, a collimator system, step motors, and a sample holder. The bremsstrahlung component of the X-ray source (a standard tungsten tube, used at 45 kV and 35 mA) was used.

The primary beam intensity $I_0(E)$ was directly measured by using the same voltage (45 kV) and reducing the tube current to 2 mA at the zero scattering angle without sample. The

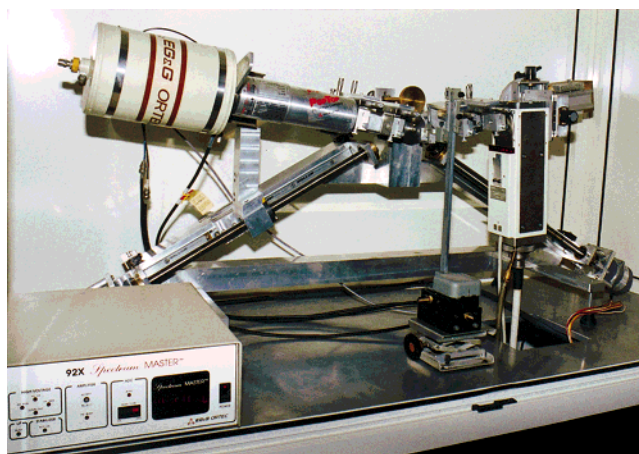


Figure 1. Photo of the energy dispersive X-ray noncommercial diffractometer, Dipartimento di Chimica, Istituto Nazionale di Fisica della Materia, Università di Roma “La Sapienza”.

transmission of the sample was measured under the same conditions.

From the ratio

$$I_t(E)/I_0(E) = e^{-\mu(E)t}$$

we obtained the experimental $e^{-\mu(E)t}$, which was used in eqs 6 and 7 below for the absorption corrections.¹⁹

The fluorescence lines present in the 5–11 keV range due to the W source and to the cations (Zn and Cu) do not disturb our measurements, since they are outside the region of our interest.

A Seifert and Rich high-voltage power supply with a stability better than 0.1% was used. The detecting system consists of an EG&G liquid nitrogen cooled ultrapure Ge SSD (ORTEC, Model 92X) connected to a PC via ADCAM hardware. The current pulse coming out of the detector is converted into a digital signal, which is visualized on a computer screen through a multichannel analyzer (MCA). The collimating system is composed of four adjustable width W slits purposely placed to reduce the X-ray beam angular divergence. The X-ray tube and the detecting system holding arms can rotate in the vertical plane around a common center in order to reach the desired 2θ scattering angle. Step motors, allowing reproducibility within 0.001 for the scattering angles, accomplish the movement of the arms. The diffractometer is shown in Figure 1. Measurement angles were $\theta = 26^\circ, 21^\circ, 15.5^\circ, 10.5^\circ, 8.0^\circ, 5.0^\circ, 3.5^\circ, 3.0^\circ, 2.0^\circ, 1.5^\circ, 1.0^\circ, 0.5^\circ$, and they supply a scattering parameter interval q of $0.15\text{--}18.325 \text{ \AA}^{-1}$ ($q = [4\pi/hc]E \sin \theta$).

The total intensity \tilde{I} scattered by the sample and measured by an energy dispersive detector in approximation of single scattering and transmission geometry can be expressed as

$$\tilde{I}(E, \theta) = KI_0(E) P(E, \theta) A_{\text{Coh}}(E, \theta) I(E, \theta) \quad (1)$$

with

$$I(E, \theta) = I_{\text{Coh}}(E, \theta) + \frac{E'I_0(E') P(E', \theta) A_{\text{Inc}}(E, E', \theta) I_{\text{Inc}}(E', \theta)}{EI_0(E) P(E, \theta) A_{\text{Coh}}(E, \theta)} \quad (2)$$

where θ is the scattering angle, E is the photon energy recorded by the detector, and E' is the initial energy of a photon scattered inelastically and observed at the energy E .

From Compton's incoherent scattering, we have the expression

$$E' = E \left(\frac{2E \sin^2 \theta}{mc^2} \frac{1}{1 - \left(\frac{2E \sin^2 \theta}{mc^2} \right)} \right) \quad (3)$$

K is the scale factor between the intensity reaching the detector and the intensity scattered by a stoichiometric unit of the sample. $I_0(E)$ is the energy spectrum of the primary beam measured at $\theta = 0^\circ$. $P(E, \theta)$ is the polarization factor by a scattering of a primary radiation with polarization $\Phi(E)$ that is

$$P(E, \theta) = (1 + \cos^2 2\theta)/2 + \sin^2 2\theta \Phi(E)/2 \quad (4)$$

with

$$\Phi(E) = [I_{p,n}(E) - I_{p,p}(E)]/[I_{p,n}(E) + I_{p,p}(E)] \quad (5)$$

where $I_{p,n}$ and $I_{p,p}$ are intensities of the normal and parallel polarization components, respectively, with respect to the scattering plane.

$A_{\text{Coh}}(E, \theta)$ is the X-ray elastic absorption coefficient:

$$A_{\text{Coh}}(E, \theta) = \exp[-\mu(E)t \sec \theta] \quad (6)$$

$A_{\text{Inc}}(E, E', \theta)$ is the X-ray inelastic absorption:

$$A_{\text{Inc}}(E, E', \theta) = \frac{\exp[-\mu(E)t \sec \theta] - \exp[-\mu(E')t \sec \theta]}{-\mu(E)t \sec \theta [-\mu(E')t \sec \theta]} \quad (7)$$

After correction of the experimental data for the escape peak suppression, the intensity data were handled by means of our DIF1 program written in FORTRAN. This program also made the necessary absorption corrections to combine the sets of data taken at different angles, as described in the paper of Nishikawa and Iijima.¹⁹

Normalization to a stoichiometric unit of volume containing one metal atom was performed: normalized concentrations are reported in Table 1.

Radial distribution functions, $D(r)$, were calculated from the static structure functions $i(q)$:

$$i(q) = I_{\text{Coh}}(E, \theta) - \sum_n c_n f_n^2(q) \quad (8)$$

according to the expression

$$D(r) = 4\pi r^2 \rho_0 + 2r/\pi \int_0^{q_{\text{max}}} qi(q) M(q) \sin(qr) dq \quad (9)$$

In this equation $\rho_0 = [\sum_i n_i f_i(0)]^2/V$, where V is the stoichiometric volume of chosen unit, n_i is the number of atoms i per unit volume, and f_i is the scattering factor per atom i .

$$M(q) = [f_{\text{Zn}}^2(0)/f_{\text{Zn}}^2(q)] \exp(-0.01q^2)$$

is the sharpening factor. As the upper integration limit, we chose $q_{\text{max}} = 18.325 \text{ \AA}^{-1}$.

Theoretical peaks were calculated by a corresponding Fourier transform of the theoretical structure-function for pairs of interactions (Debye function):

$$i_{\text{pq}}(q) = \sum f_p f_q \sin(r_{\text{pq}} q) (r_{\text{pq}} q)^{-1} \exp(-1/2\sigma_{\text{pq}}^2 q^2) \quad (10)$$

using the same sharpening factor and the same q_{max} value as for the experimental data and assuming the root mean square

TABLE 2: Metal–Oxygen Distances (r), Number of Nearest Neighbors (n), and Standard Deviation (σ) Used for All the Samples

M	R (Å)	n	σ (Å)
Zn	2.13	6	0.11
Mg	2.09	6	0.11
Cu _p	1.93	4	0.09
Cu _a	2.30	2	0.11

(rms) variation in interatomic distance to be σ_{pq} . These values are reported in Table 2.

Results and Discussion

1. Conductivity. The conductivity of the solutions was determined in order to ascertain their possible use as electrolyte media. The Arrhenius plots of the solutions were determined by following the impedance response of symmetrical cells at different temperatures. The results are reported in Figure 2. The

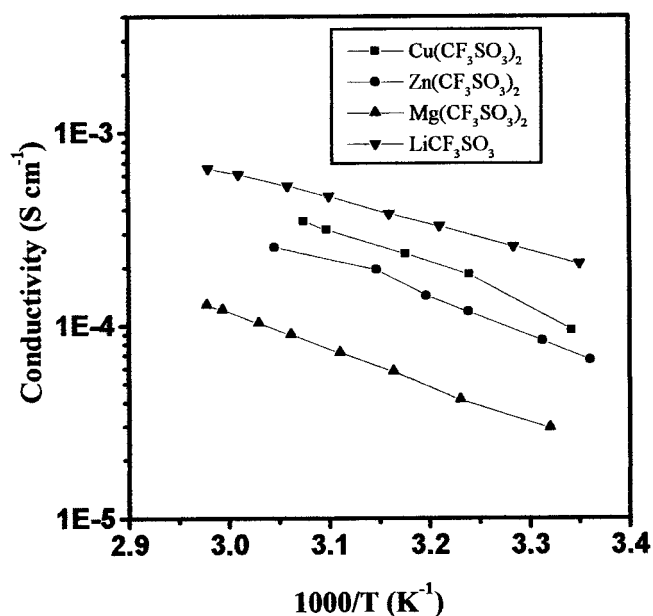


Figure 2. Conductivity of symmetrical cells at different temperatures (Arrhenius plot) for the PEGM-based systems.

conductivity trends approach the curvature typical of amorphous phases.

The conductivity in these systems is lower than the corresponding Li-based electrolyte, which may be a consequence of the high ionic charge on the cations causing restrictions on chain dynamics through transient cross-links.

Over the whole temperature range, the Cu solution shows the best characteristics. This behavior can be related to the hardness of the divalent cations, since harder cations show a larger conductivity. Because of similar donicities of the oxygen in water and in ethers, exchange rates can be expected to follow a similar trend. The exchange rate of solvent coordinated to a cation is affected by many factors such as cation radius and charge, though for the metal cations more specific electronic effects are often dominant.

Among divalent-cation-based systems, those containing mercury cations show very reasonable conductivity levels, not dissimilar to those found for lithium systems and much higher than other divalent-cation-based systems.^{20,21} On the basis of the hard-soft classification of acid and bases, the hardness of the divalent cations follows the trend $\text{Mg}^{2+}, \text{Ca}^{2+} > \text{Ni}^{2+}, \text{Cu}^{2+}, \text{Zn}^{2+}, \text{Co}^{2+}, \text{Pb}^{2+} > \text{Cd}^{2+}, \text{Hg}^{2+}$.

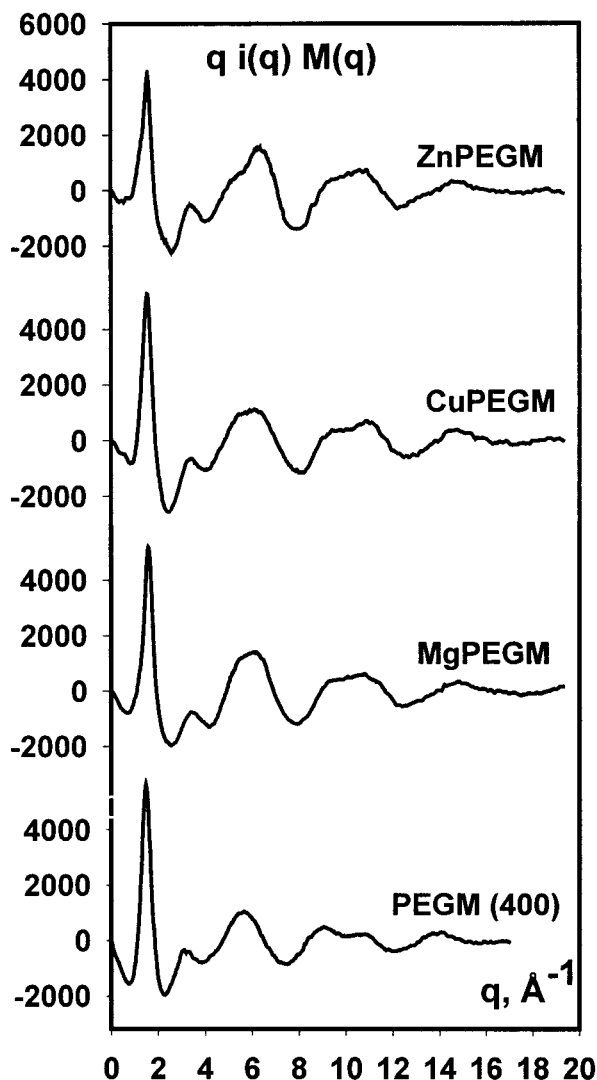


Figure 3. Structure function, $qi(q)M(q)$ for the PEGM(400) solutions, with $\text{Zn}(\text{CF}_3\text{SO}_3)_2$, $\text{Cu}(\text{CF}_3\text{SO}_3)_2$, and $\text{Mg}(\text{CF}_3\text{SO}_3)_2$ salts and pure PEGM(400)

As Hg^{2+} is a soft cation, much weaker interactions would be expected with the hard ether-oxygen-coordinating group than Mg^{2+} or Ca^{2+} would experience. Consequently, Hg^{2+} would be expected to be mobile, while Mg^{2+} or Ca^{2+} would be immobile.

Measured transference numbers for cations other than lithium show some interesting features. Notably, Mg^{2+} appears to be immobile while Hg^{2+} has a transference number close to that of alkali metals, despite carrying the same charge. These results have been brought together through a comparison of cation transference numbers and water exchange rates around aqueous cations, as determined by Eigen.²² An essential prerequisite for significant cation mobility appears to be a high lability of the cation-polymer bond. Thus, while strong cation-polymer bonds are necessary for polymer electrolyte formation, labile bonds are necessary for cation mobility.

2. X-ray Structure Determination. In Figure 3 the structure function in the form $qi(q)M(q)$ of the three solutions and pure PEGM(400) are reported. The curves all display a similar oscillation period and amplitude, indicating that the solutions structure is not significantly altered by the presence of the cations. In Figure 4 the correlation functions, in the form $\text{Diff}(r) = [D(r) - 4\pi r^2 \rho_0]$, for solutions and pure solvent are reported.

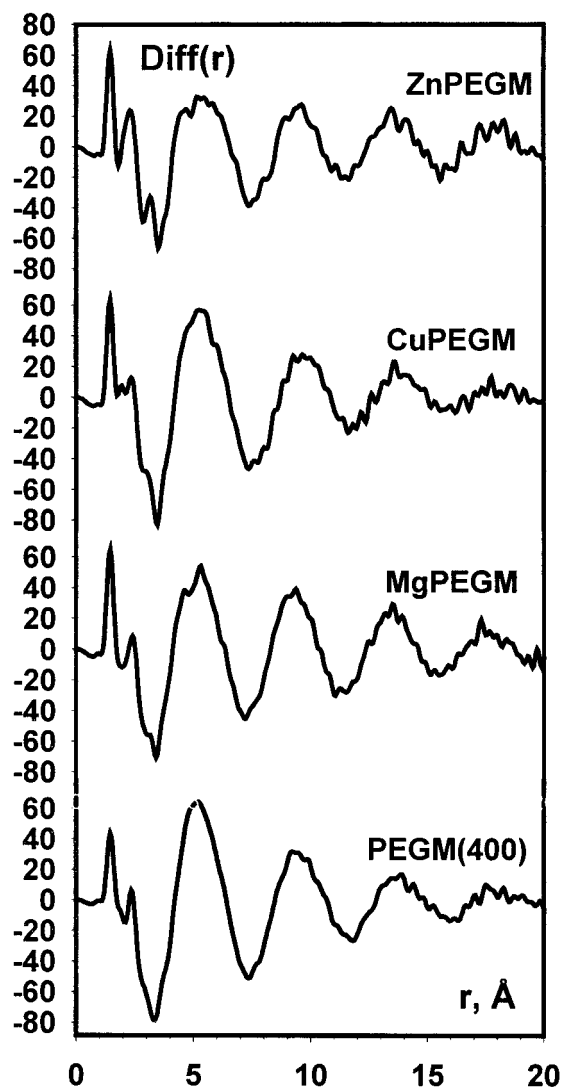


Figure 4. Correlation functions, $\text{Diff}(r) = [D(r) - 4\pi r^2 \rho_0]$, for the PEGM(400) solutions, with $\text{Zn}(\text{CF}_3\text{SO}_3)_2$, $\text{Cu}(\text{CF}_3\text{SO}_3)_2$, and $\text{Mg}(\text{CF}_3\text{SO}_3)_2$ salts and pure PEGM(400).

Similarly, we do not observe sensible differences when three different cations are present in the PEGM solution. Particularly, the presence of the cations does not affect the long-range structure, where the solvent-solvent interactions dominate, but there are some small differences in the short-range main peaks, common to three solutions, which will be minutely discussed.

The contributions due to the triflate ion intermolecular interactions, with geometry obtained by theoretical calculations, and to the PEGM oligomeric unity intermolecular interactions have been subtracted from the experimental $D(r)$ of the three solutions. A model chain has been considered for the PEGM. The 1-4 atom interaction distances may vary between 2.51 \AA and 3.73 \AA , following the configuration cis or trans. Since such distances may concern the metal coordination peak, the configuration that better represents the first and the second peak of the pure liquid has been chosen.

Hence, the metal coordination peak has been isolated; see Figure 5a-c. The coordination number has been determined to be six, the M-O distances are respectively 2.09 and 2.13 \AA for Mg and Zn; also, the Cu ion is hexacoordinated, but it has four bonds Cu-O at 1.93 \AA and two at 2.30 \AA , Figure 6a-c.

The presence of the cations does not alter very much the pure solvent's local structure. It allows us to analyze the structure

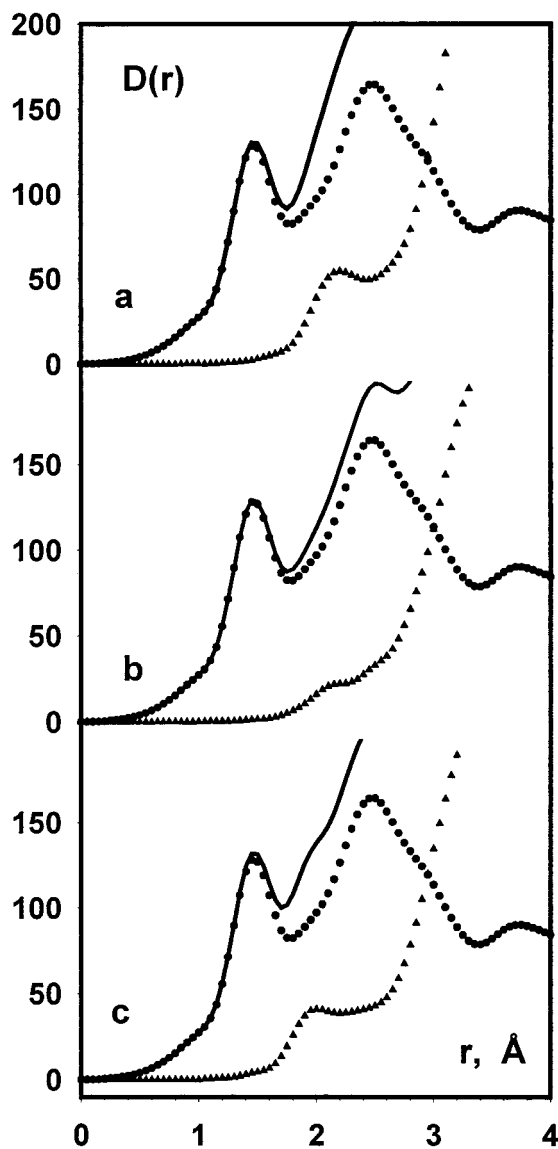


Figure 5. Experimental correlation functions $D(r)$ (—), the theoretical peak shape function for triflate and PEGM (400) (●), and their difference (▲): (a) $\text{Zn}(\text{CF}_3\text{SO}_3)_2$ PEGM (400) solution; (b) $\text{Mg}(\text{CF}_3\text{SO}_3)_2$ PEGM (400) solution; (c) $\text{Cu}(\text{CF}_3\text{SO}_3)_2$ PEGM (400) solution.

by the difference method, i.e., by subtracting the $D(r)$ curves of two different solutions, if the cation concentration is the same in both cases. The resulting curve isolates the cation–cation and cation–solvent interactions and is free from the solvent–solvent contributions.

We analyzed the curves by subtracting each pair of $D(r)$; hence, the resulting difference curves are $D(r)_{\text{Zn}} - D(r)_{\text{Mg}}$, $D(r)_{\text{Cu}} - D(r)_{\text{Mg}}$, and $D(r)_{\text{Zn}} - D(r)_{\text{Cu}}$. The difference curves of the experimental $D(r)$ were compared to theoretical peak shapes.

In Figure 7a the Zn–PEGM and Mg–PEGM $D(r)$ are reported and their difference is plotted in Figure 7b. Similarly, in Figure 8a the Cu–PEGM and Mg–PEGM $D(r)$ are reported; their difference is plotted in Figure 8b. The third pair of $D(r)$, in Figure 9a,b, represents Zn–PEGM and Cu–PEGM $D(r)$ and their difference, respectively.

First we analyze the first peak of the curves. It gives information on the metal–first neighbor interaction, i.e., a metal–oxygen interaction (it is very unlikely that the metal binds through a carbon atom), and, hence, on the coordination of the cations.

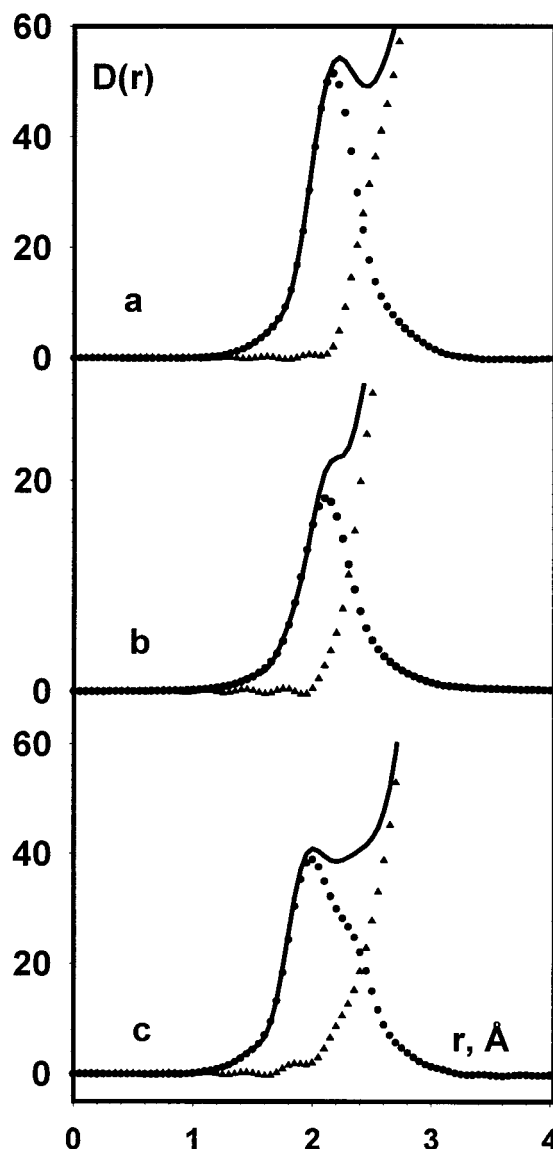


Figure 6. Difference between the correlation functions $D(r)$ and the theoretical peak shape function for triflate and PEGM (400) (—), the peak shape function of M–O interactions (●), and their difference (▲): (a) $\text{Zn}(\text{CF}_3\text{SO}_3)_2$ PEGM (400) solution; (b) $\text{Mg}(\text{CF}_3\text{SO}_3)_2$ PEGM (400) solution; (c) $\text{Cu}(\text{CF}_3\text{SO}_3)_2$ PEGM (400) solution.

The difference curve plotted in Figure 7b shows two main peaks at 2.1 and 3.2 Å, each of them with a shoulder at larger distances (2.6 and 3.7 Å, respectively).

Contributions of six metal–oxygen interactions, at slightly different lengths (2.09 Å for Mg and 2.13 Å for Zn), reproduce the first peak at 2.1 Å. The metal coordination number has been determined by studying the $D(r)$ separately and by studying the difference curve. In both cases, we find the same coordination for the two cations at the same distance. Another indication of the coordination number is given by the absence of negative peak in the difference curve. Mg is a typically hexacoordinated cation and the difference curve immediately gives information on the coordination of the cation, which is compared to it. Zn can be either hexacoordinated or tetra-coordinated, but in the latter case, the difference of the coordination would yield a negative peak of the difference $D(r)$. The positive peak in the difference curve of the Mg–PEGM and Zn–PEGM $D(r)$ is strictly correlated to the different number of scattering electrons that the two cations have.

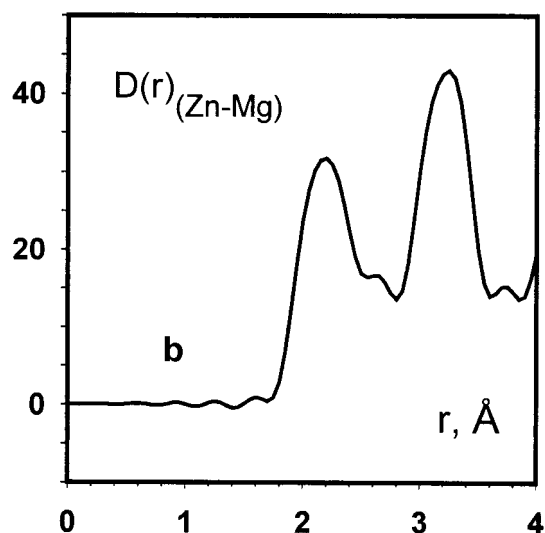
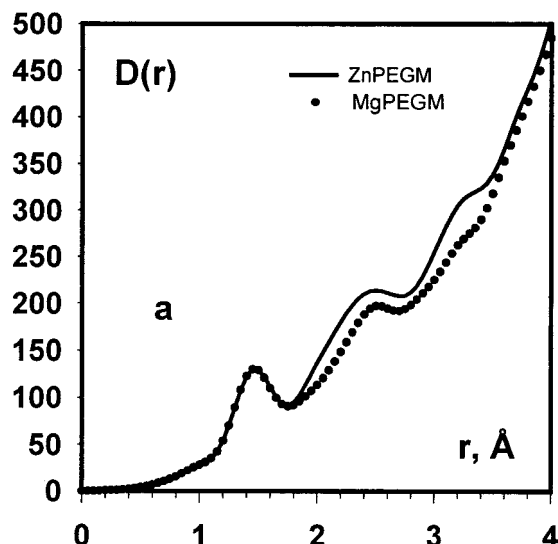


Figure 7. (a) Zn-PEGM $D(r)$ (—) and Mg-PEGM $D(r)$ (●). (b) Curve difference obtained.

The difference curve between Cu-PEGM and Mg-PEGM $D(r)$ (Figure 8b) reveals, instead, a slightly different coordination. In this case, we have to consider both peaks at 1.93 and 2.3 Å, which have almost similar intensity and are both typical figures of a first coordination sphere. The two evident peaks are fitted by two different Cu-O lengths: four distances at 1.93 Å and two distances at 2.3 Å. Cu is known to display a Jahn-Teller effect. There are two opposite bonds of the octahedron coordination, either larger or shorter lengths compared to the remaining four planar ones. In this case we could clearly observe this effect; since it would be impossible to fit the first peak at 1.93 Å with six Cu-O bonds, it would be largely overestimated.

The bond distances we have obtained for Mg(II), Zn(II), and Cu(II) in PEGM solutions can be tested by analyzing the third difference curve reported in Figure 6b. It is evident that Cu has a distorted octahedral coordination. The difference curve between the Zn-PEGM and the Cu-PEGM $D(r)$ yields a negative peak exactly at 1.93 Å; in Figure 8b we observed this peak as positive since we were subtracting a curve from $D(r)_{\text{Cu}}$. However, we compared the difference experimental $D(r)$ to a theoretical peak shape calculated with the parameters we obtained in the first two curves and we found a very good agreement. Therefore, we can conclude that both Zn(II) and Mg(II) have an octahedral symmetry in a PEGM solution at bond

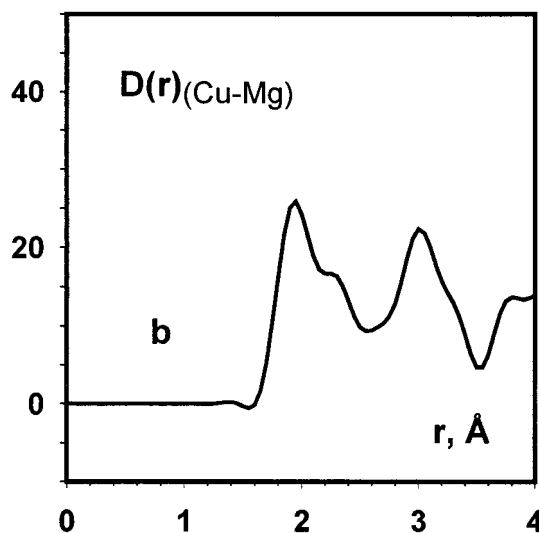
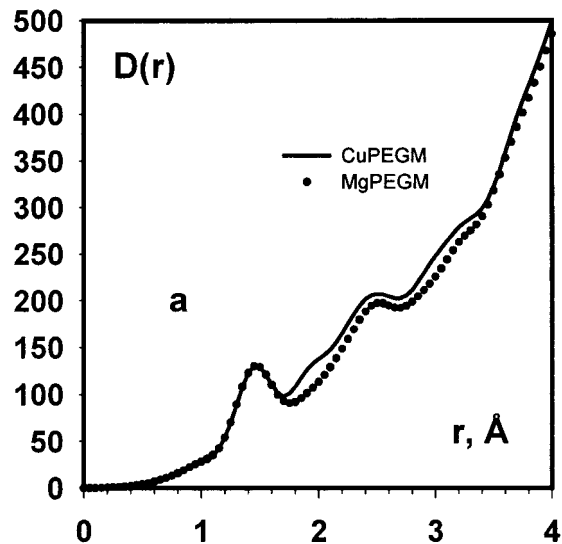


Figure 8. (a) Cu-PEGM $D(r)$ (—) and Mg-PEGM $D(r)$ (●). (b) Curve difference obtained.

distances of 2.13 and 2.09 Å, respectively. Cu(II) has a slightly distorted symmetry with four planar bonds at 1.93 Å and two apical bonds at 2.3 Å.

To analyze how the polymer chain is bonded to the different cations, we have analyzed the $D(r)$ at larger distances.

The octahedral coordination obtained with six oxygen atoms, coming from PEG, implies a second coordination sphere formed by twelve M-C contributions. Considering an isomorphous conformation for Zn and Mg, the second sphere reproduces exactly the second peak in the difference curve at 3.2 Å. It does not provide any information about the O atoms involved in the coordination. They may be in any point of the chain and may come from one chain or from more chains, and they are always bonded to two C atoms.

The length of the chains would allow a single chain to tie an M atom, but the models where two consecutive oxygens are used result in large steric strain. To understand how many chains coordinate the metal ion, we can take into account that the ratio metal/polymer chains is 1/2, and assume that, on average, two polymer chains are bonded to one cation.

An aid to determine this geometry comes from the examination of peaks successive to the second peak. The modest height of the peak successive to 4.0 Å imposes a limited number of contributions in this area. This implies that three oxygen atoms

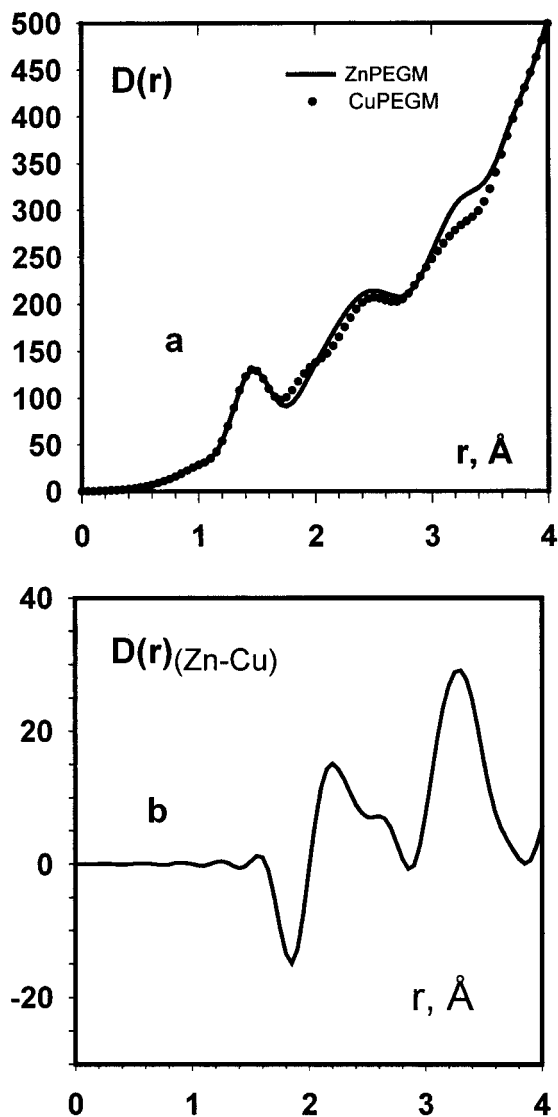


Figure 9. (a) Zn-PEGM $D(r)$ (—) and Cu-PEGM $D(r)$ (●). (b) Curve difference obtained.

of the same polymer chain are bonded to the metal atom, 6 being the coordination number of Mg and Zn. The polymer chain has eight monomer units, i.e., nine oxygen atoms available for the coordination. The oxygen atoms have many possible ways to bind the metal, but we can restrict them.

Two of the three O atoms must be the O terminals that drive to the extremity a CH_3 group only. Thus, the two extremities do not provide contributions beyond the second coordination sphere.

The O that ties the third site could be the fourth or the fifth. If the third or the second oxygen were interested in the bond, the chain could not depart enough and the contributions before 5.0 Å would be too large.

For the two isomorphous systems, a model has been proposed. The PEGM O atoms involved in the metal coordination are 1° – 5° – 9° , considering the coordination of the central O atom in a PEGM (400) with an average length chain of eight monomer units. In Figure 10 the possible model for coordination in the $\text{Mg}(\text{CF}_3\text{SO}_3)_2$ is shown.

As far as the solution containing copper is concerned, if we consider its difference curves with Mg and Zn, we notice that it is not isomorphous to the other two. The only structural information that we can obtain for this solution comes exclu-

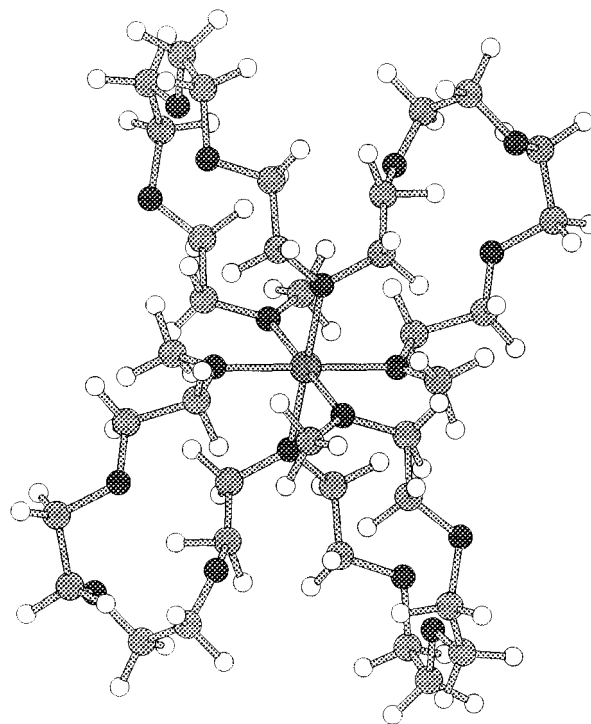


Figure 10. Possible model for coordination in the Mg-PEGM system.

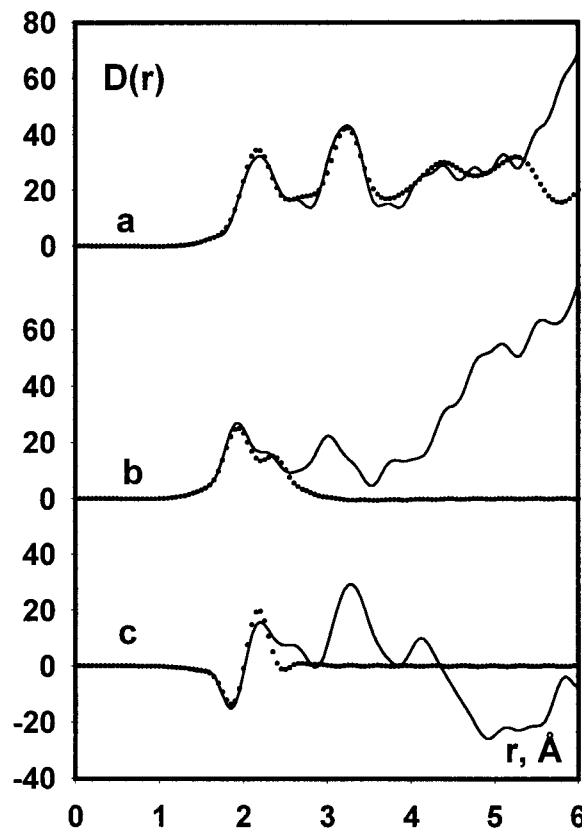


Figure 11. (a) (Zn-Mg) experimental difference curve (—), theoretical peak shape difference of the proposed model, for Zn-PEGM and Mg-PEGM solutions (●). (b) (Mg-Cu) experimental difference curve (—), the theoretical peak shape difference of the interactions M-O in Mg-PEGM and Cu-PEGM solutions (●). (c) (Zn-Cu), experimental difference curve (—), and the theoretical peak shape difference of the interactions M-O in Cu-PEGM and Mg-PEGM solutions (●).

sively from the first peak. The three experimental difference curves are compared with the theoretical peak shape difference curves in Figure 11. In Figure 11a, the difference curve, between

Zn and Mg solutions, is compared with the theoretical curve obtained from the total model. In Figure 11b,c the two other difference curves are compared with the theoretical ones, obtained from the theoretical first peaks differences, regarding the Cu solution.

If the Cu solution had been isomorphous to the other ones as far as its difference with that of Mg is concerned, we would have obtained a difference curve like the Zn–Mg curves.

The curve should have a course similar to the former. The Zn–Cu difference curve would have to show a parabolic curve, due to the electronic difference between Zn–Cu. Small oscillations, due to the differences of bond length, as happens for the first peak, can be present. A negative peak is in effect obtained at 1.93 Å interaction length at the plain level and a positive peak at 2.13 Å, which corresponds to the Zn–O interaction distance.

Conclusions

In this work, PEGM (400) solutions with Zn(II), Mg(II), and Cu(II) triflate salts have been compared. The solutions containing Zn and Mg were found to be very similar in their coordination and conformation. The dissolution of $\text{Zn}(\text{CF}_3\text{SO}_3)_2$ and $\text{Mg}(\text{CF}_3\text{SO}_3)_2$ in PEGM (400) gives rise to isomorphous solutions; the metal ions reach an octahedral conformation by six ether oxygens of the polymer chains.

On the dissolution of $\text{Cu}(\text{CF}_3\text{SO}_3)_2$, into the polymer, a coordination of six ether oxygens, in a bipyramidal geometry, for each Cu, is obtained. The polymer chain seems to have a different behavior, giving rise to a solution nonisomorphous to the other metal ion ones.

References and Notes

(1) Scrosati, B. In *Application of Electroactive Polymers*; Scrosati, B., Ed.; Chapman and Hall: London, 1993; p 21.

- (2) Sadaoka, Y.; Sakai, Y.; Akiyama, H. *J. Mater. Sci.* **1986**, *21*, 235.
- (3) Fabry, P.; Montero-Ocampo, C.; Armand, M. *Sens. Actuators* **1988**, *15*, 1.
- (4) Jensen, J. In *Fuel Cells: Trends in Research Applications*; Appleby, A. J., Ed.; Hemisphere: New York, 1987; p 145.
- (5) Appleby, A. J. In *Fuel Cells: Trends in Research Applications*; Appleby, A. J., Ed.; Hemisphere: New York, 1987; p 19.
- (6) Gray, F. M. *Solid Polymer Electrolytes, Fundamentals and Technological Application*; VCH: New York, 1991.
- (7) Hooper, A.; Gauthier, M.; Belanger, A. In *Electrochemical Science and Technology of Polymers*; Linford, R. G., Ed.; Elsevier: London, 1990; p 375.
- (8) Gauthier, M.; Belanger, A.; Kapfer, B.; Vassort, G.; Armand, M. In *Polymer Electrolyte Reviews*; MacCallum, R. J., Vincent, C. A., Eds.; Elsevier: New York, 1989; p 285.
- (9) Scrosati, B.; Neat R. J. In *Application of Electroactive Polymers*; Scrosati, B., Ed.; Chapman and Hall: London, 1993; p 182.
- (10) Bruce, P. G. *Electrochim. Acta* **1995**, *40* (13–14), 2086.
- (11) Yang, H. Farrington, G. C. In *Second International Symposium on Polymer electrolytes*; Scrosati, B., Ed.; Elsevier: New York, 1989; p 265.
- (12) Bernson, A.; Lindgren, J.; Huang, W.; Frech, R. *Polymer* **1995**, *36* (23), 4471.
- (13) Druger, S. D.; Nitzan, A.; Ratner, A. M. *J. Chem. Phys.* **1983**, *79*, 3133.
- (14) Shi, J.; Vincent, C. A. *Solid State Ionics* **1993**, *60*, 11.
- (15) Ratner, A. M. *Faraday Discuss. Chem. Soc.* **1989**, *88*, 91.
- (16) Caminiti, R.; Cilloco, F.; Felici, R. *Mol. Phys.* **1992**, *76*, No. 3, 681.
- (17) Caminiti, R.; Sadun, C.; Rossi, V.; Cilloco, F.; Felici, R. XXV Italian Congress of Physical Chemistry, Cagliari, Italy, 1991.
- (18) Caminiti, R.; Sadun, C.; Rossi, V.; Cilloco, F.; Felici, R. Patent No. 01261484, 1993.
- (19) Nishikawa, K.; Iijima, T. *Bull. Chem. Soc. Jpn.* **1984**, *57*, 750.
- (20) Shi, J. Vincent, C. A. *Solid State Ionics* **1993**, *60*, 11.
- (21) Bruce, P. G.; Krok, F. C.; Vincent, A. *Solid State Ionics* **1988**, *27*, 81.
- (22) Eigen, M. *Pure Appl. Chem.* **1963**, *6*, 97.